

# Multidimensional Discretization of the Stationary Quantum Drift-Diffusion Model for Ultrasmall MOSFET Structures

Shinji Odanaka, *Senior Member, IEEE*

**Abstract**—This paper describes a new approach to construct a multidimensional discretization scheme of quantum drift-diffusion (QDD) model (or density gradient model) arising in MOSFET structures. The discretization is performed for the stationary QDD equations replaced by an equivalent form, employing an exponential transformation of variables. A multidimensional discretization scheme is constructed by making use of an exponential-fitting method in a class of conservative difference schemes, applying the finite-volume method, which leads to a consistent generalization of the Scharfetter–Gummel expression to the nonlinear Sturm–Liouville type equation. The discretization method is evaluated in a variety of MOSFET structures, including a double-gate MOSFET with thin body layer. The discretization method provides numerical stability and accuracy for carrier transport simulations with quantum confinement effects in ultrasmall MOSFET structures.

**Index Terms**—Density gradient theory, discretization, double-gate MOSFET, MOSFET, quantum confinement, quantum drift-diffusion (QDD) model, semiconductor transport.

## I. INTRODUCTION

THE development of new MOSFET structures into the 10-nm regime, which includes aggressively scaled MOSFETs with high-dielectric-constant gate dielectric, ultrathin body silicon-on-insulator (SOI) devices, double-gate MOSFETs, and FinFETs [1], is an attractive challenge to improve circuit performance in the future integrated system. The performance of such ultrasmall MOSFETs primarily depends on the quantum mechanical effects. This creates the need of a numerical device model available for the computer-aided design of ultrasmall MOSFETs. It has been shown that the quantum drift-diffusion model (or density-gradient model), which is derived from the density-gradient theory based on thermodynamical grounds [2] and Wigner function technique [3], is suited to incorporate quantum confinement and tunneling effects in MOSFET structures [5]. Moreover, this model is of physical and practical importance for carrier transport modeling in multidimensional MOSFET structures, as a generalization of the classical drift-diffusion model. The multidimensional discretization of the quantum drift-diffusion (QDD) model is a major concern to achieve high computational capability of current-voltage characteristics for a variety of MOSFET structures.

In such a numerical modeling of MOS transport, however, some studies have pointed out numerical difficulties of a coarse grid, convergence at high drain biases and strong sensitivity to initial guesses [6], [8], [11]. Recently, a few papers discuss numerical approach to construct an iterative solution method and discretization schemes to the QDD equations [6]–[9].

The purpose of this paper is to describe a multidimensional discretization scheme of the stationary QDD model arising in MOSFET structures. The discretization is performed for the stationary QDD equations replaced by an equivalent form, employing the exponential transformation of variables. A multidimensional scheme is constructed in terms of a new set of unknown variables, applying the finite-volume method. The discretization method is evaluated in a variety of ultrasmall MOSFET structures. Section II discusses a quantum drift-diffusion model with emphasis on numerical modeling of the coupled equation system. Section III describes a multidimensional discretization scheme of the stationary QDD model, yielding a conservative scheme using an exponential-fitting method. Such a scheme was first developed for the QDD equation (or Density-gradient equation) in one dimension by Ancona *et al.* [8], [9]. A comparison of previous work is further discussed. In Section IV, the numerical results are verified to evaluate the discretization method, comparing with those calculated from the Schrödinger equation coupling with Poisson equation and a classical drift-diffusion model. The carrier transport simulations with quantum confinement effects in a double-gate MOSFET are demonstrated.

## II. QDD MODEL

For the modeling of ultrasmall semiconductor devices, the QDD model, which is also called the density-gradient model, was proposed by Ancona *et al.* in the density-gradient theory [2], [3]. This model is a quantum corrected version of the classical drift-diffusion model, with  $O(\hbar^2)$  corrections to the stress tensor, and is viewed as one of the hierarchy of the quantum hydrodynamic models [4]. The expression for the quantum potentials  $\gamma_n$  and  $\gamma_p$  for electrons and holes, which are related to the quantum corrected stress tensor, was derived as follows:

$$\gamma_n = 2b_n \frac{\nabla^2 \sqrt{n}}{\sqrt{n}} \quad (1)$$

$$\gamma_p = 2b_p \frac{\nabla^2 \sqrt{p}}{\sqrt{p}} \quad (2)$$

Manuscript received September 11, 2003; revised December 3, 2003. This paper was recommended by Associate Editor Z. Yu.

The author is with the Computer Assisted Science Division, Cybermedia Center, Osaka University, Toyonaka, Osaka 560-0043, Japan (e-mail: odanaka@cmc.osaka-u.ac.jp).

Digital Object Identifier 10.1109/TCAD.2004.828128

where  $n$  and  $p$  are the electron and hole densities. The density-gradient coefficients for electrons and holes are  $b_n = \hbar^2/(12qm_n^*)$  and  $b_p = \hbar^2/(12qm_p^*)$ , respectively, where  $m_n^*$  and  $m_p^*$  are effective masses for the electrons and holes, and  $\hbar$  is the Planck constant. The current continuity equations of the QDD model yield the fourth-order equations for the electron and hole densities, respectively. The stationary QDD equations are described in divergence form, adding the recombination rate. For Boltzmann statistics, the continuity equations then become

$$\nabla \left( \mu_n n \nabla \left( \varphi - \frac{kT}{q} \log \left( \frac{n}{n_i} \right) + \gamma_n \right) \right) + R = 0 \quad (3)$$

$$-\nabla \left( \mu_p p \nabla \left( \varphi + \frac{kT}{q} \log \left( \frac{p}{n_i} \right) - \gamma_p \right) \right) + R = 0 \quad (4)$$

where  $\mu_n$  and  $\mu_p$  are electron and hole mobilities, and  $n_i$  is the intrinsic density.  $k$  is the Boltzmann constant and  $T$  is the carrier temperature.  $R$  is the recombination rate. The current continuity equations, (3) and (4), are self-consistently coupled to the Poisson equation for the electrostatic potential  $\varphi$ . In a simulation region  $\Omega$ , the QDD model is solved, supplementing appropriate boundary conditions on a boundary  $\partial\Omega$ .

Since the current continuity equations of the QDD model are the fourth-order equation for the electron and hole densities, there is no maximum principle available for constructing a well-defined solution map associated with the coupled system and the derivation of numerical scheme requires discretization of a higher order differential operator.

It is suggested that the fourth-order equations, (3) and (4), can be rewritten by two second-order equations, respectively, by introducing the generalized chemical potentials [2], [6]

$$\varphi_n = \varphi - \frac{kT}{q} \log \left( \frac{n}{n_i} \right) + \gamma_n \quad (5)$$

and

$$\varphi_p = \varphi + \frac{kT}{q} \log \left( \frac{p}{n_i} \right) - \gamma_p. \quad (6)$$

In this view, the current continuity (3) for electrons is split into the following second-order equation, which requires the positivity of solutions  $S_n = \sqrt{n}$  from the mathematical point of view:

$$2b_n \nabla^2 S_n - \gamma_n S_n = 0 \quad (7)$$

and the continuity equation in terms of the generalized chemical potential

$$\nabla(\mu_n n \nabla \varphi_n) + R = 0. \quad (8)$$

A similar expression is obtained for the holes. As a result, the equation system of the stationary QDD model is expanded to five second-order elliptic equations, including the Poisson equation. When  $\gamma_n = 0$  holds in the simulation region  $\Omega$ , the QDD (3) for electrons reduces to a classical drift-diffusion equation. In the coupled system of (7) and (8), this case leads to the sin-

gular solutions to the Helmholtz equation (7) and, hence, numerical solutions of the classical DD model are not good initial guesses for solving the QDD model. When the drain bias is applied, the quantum potential  $\gamma_n$  is further sensitive to the variation of the chemical potentials. It has been pointed out in MOSFET simulations that convergence with the coupled system is difficult at high drain bias [6].

Choice of the unknown variables is an important issue to solve the expanded equation system of the QDD model. A set of the five unknown variables has to be discussed from the physical point of view and numerical reasons. In most of previous works [5], [6], [8], [12], the coupled equation system (7) and (8) was solved for in terms of the unknown variables  $\varphi$ ,  $\sqrt{n}$ ,  $\sqrt{p}$  and  $\varphi_n$ ,  $\varphi_p$ , coupling with the Poisson equation. In an alternative approach [10], the choice of unknown variables  $\varphi$ ,  $\Phi_n = \varphi + \gamma_n$ ,  $\Phi_p = \varphi - \gamma_p$  and  $n$ ,  $p$  was proposed with model modification in the insulators for the numerical implementation of the DG model, assuming that the insulators are a wide band gap semiconductor [10], [11].

In this work, we introduce a new approach to construct a discretization scheme of the QDD model by a set of unknown variables  $\varphi$ ,  $u_n$ ,  $u_p$ , and  $\varphi_n$ ,  $\varphi_p$ , where  $u_n = ((\varphi + \gamma_n - \varphi_n)/2)$  and  $u_p = ((\varphi_p + \gamma_p - \varphi)/2)$ , assuming Boltzmann statistics. Numerical implementation of Fermi–Dirac statistics is briefly discussed in the Appendix. Using the variable  $u_n$ , the electron density is rewritten as

$$S_n = \sqrt{n} = \sqrt{n_i} e^{u_n} \quad (9)$$

where all of potentials are scaled by the Boltzmann voltage  $kT/q$ . By employing an exponential transformation of variables  $S_n = \sqrt{n_i} e^{u_n}$ , (7) is replaced by the equivalent form

$$-b_n \nabla(S_n \nabla u_n) + S_n u_n = \frac{S_n}{2}(\varphi - \varphi_n). \quad (10)$$

When the variables  $\varphi$ ,  $\varphi_n$ , and  $S_n$  are given, the general Sturm–Liouville type equation, (10), is solved in silicon subject to the boundary conditions for  $u_n$ . The boundary condition at contacts is given by  $u_n = \varphi_b/2$ , assuming  $\gamma_n = 0$  at Ohmic contacts, where  $\varphi_b$  is the built-in voltage. At open boundaries, the normal derivative vanishes,  $(\partial u_n / \partial \nu) = 0$ . The boundary condition of  $u_n$  on the silicon/oxide interface is given by assuming a small constant carrier density. The discretization of the electron current continuity equation in space is performed for two equations, (8) and (10). In this approach, a numerical advantage of (10) is to ensure that the approximation of the electron density is strictly positive, if the variable  $u_n$  is uniformly bounded in  $\Omega$ . The diffusion and absorption coefficients in (10) are maintained to be positive, while the coefficient  $S_n$  exhibits the exponential nonlinearity.

### III. DISCRETIZATION SCHEME

The Sturm–Liouville-type equation, (10), with the exponential behavior of the coefficient  $S_n$  is discretized by a conservative difference scheme, which was obtained by Tikhonov and Samarskii for equations with discontinuous coefficients [13], applying the finite-volume method to construct a multidimensional scheme.

The simulation region  $\Omega$  is partitioned into computational cells  $\Omega_i$ , i.e.,  $\Omega = \cup_i \Omega_i$ . Assuming that the flux  $F = S_n \nabla u_n$  in (10), we obtain by Green's formula over each computational cell  $\Omega_i$  that

$$\int_{\partial\Omega_i} b_n S_n \frac{\partial u_n}{\partial \nu} ds - \int_{\Omega_i} S_n u_n dx = -\frac{1}{2} \int_{\Omega_i} S_n (\varphi - \varphi_n) dx \quad (11)$$

where  $\nu$  denotes the unit outward normal to the boundary  $\partial\Omega_i$  of the computational cell. In a staggered Cartesian grid in two dimensions, where the computational cell is rectangular, and the variables  $\varphi$ ,  $\varphi_n$ ,  $u_n$ ,  $S_n$  are defined at cell centers and the flux  $F$  is defined at cell interfaces, we obtain a discrete form of (11)

$$a_j b_n \left( F_{i+\frac{1}{2}} - F_{i-\frac{1}{2}} \right) + a_i b_n \left( F_{j+\frac{1}{2}} - F_{j-\frac{1}{2}} \right) - u_{ni,j} \times \int_{y_{j-\frac{1}{2}}}^{y_{j+\frac{1}{2}}} \int_{x_{i-\frac{1}{2}}}^{x_{i+\frac{1}{2}}} S_n dx = -\frac{1}{2} (\varphi - \varphi_n)_{i,j} \int_{y_{j-\frac{1}{2}}}^{y_{j+\frac{1}{2}}} \int_{x_{i-\frac{1}{2}}}^{x_{i+\frac{1}{2}}} S_n dx, \quad (12)$$

where  $a_i$  and  $a_j$  are the cell sizes of the computational cell  $\Omega_i$ . In order to find  $F_{i+1/2}$  at cell interfaces, integrating the flux  $F$  over the interval  $[x_i, x_{i+1}]$ , an approximation  $F_{i+1/2}$  yields

$$F_{i+\frac{1}{2}} = \frac{u_{ni+1,j} - u_{ni,j}}{\int_{x_i}^{x_{i+1}} \frac{dx}{S_n}}. \quad (13)$$

A similar expression is obtained for  $F_{i-1/2}$ ,  $F_{j-1/2}$ , and  $F_{j+1/2}$ . Substituting in (12) the average fluxes  $F_{i\pm 1/2}$  and  $F_{j\pm 1/2}$  leads to a class of conservative schemes to (10) [13].

The key ingredient is an appropriate computation of the function  $S_n$  in (12) and (13). In general, the explicit integration of  $S_n$  can become very difficult. A standard centered scheme is constructed with simplified integrals

$$\int_{x_i}^{x_{i+1}} \frac{dx}{S_n} = \frac{h_{i+1}}{\sqrt{S_{ni+1,j} S_{ni,j}}} \quad (14)$$

and

$$\int_{y_{j-\frac{1}{2}}}^{y_{j+\frac{1}{2}}} \int_{x_{i-\frac{1}{2}}}^{x_{i+\frac{1}{2}}} S_n dx = S_{ni} |\Omega_i| \quad (15)$$

where  $h_{i+1} = x_{i+1} - x_i$  and  $|\Omega_i|$  is the volume of the cell. For a function  $S_n = e^{u_n}$  with the exponential behavior, an alternative explicit integration is obtained by assuming that  $du_n/dx$  is constant on the interval  $[x_i, x_{i+1}]$ . Then, we have

$$\int_{x_i}^{x_{i+1}} e^{-u_n} dx = \frac{h_{i+1} e^{-u_{ni+1,j}}}{B(u_{ni+1,j} - u_{ni,j})} \quad (16)$$

where  $B(\cdot)$  is the Bernoulli function. This expression is also derived by the Scharffeter and Gummel approach [14]. Substituting (16) into (13), the average flux  $F_{i+1/2}$  results in

$$F_{i+\frac{1}{2}} = \frac{1}{h_{i+1}} e^{u_{ni+1,j}} B(u_{ni+1,j} - u_{ni,j}) (u_{ni+1,j} - u_{ni,j}). \quad (17)$$

To obtain a high-order accurate scheme to the general Sturm–Liouville-type equation, an average of  $S_n$  in each computational cell is performed by integrating the piecewise-linear representation of  $u_n$  by

$$u_n = u_{ni,j} + \frac{\partial u_n}{\partial x} (x - x_{i,j}) + \frac{\partial u_n}{\partial y} (y - y_{i,j}) \quad (18)$$

where  $(\partial u_n / \partial x) = \text{const}$  on the intervals  $[x_{i-1/2}, x_i]$  and  $[x_i, x_{i+1/2}]$ ,  $(\partial u_n / \partial y) = \text{const}$  on the intervals  $[y_{j-1/2}, y_j]$  and  $[y_j, y_{j+1/2}]$ , respectively. Then, after some calculation we have the following approximation:

$$\Lambda_{i,j} = \int_{y_{j-\frac{1}{2}}}^{y_{j+\frac{1}{2}}} \int_{x_{i-\frac{1}{2}}}^{x_{i+\frac{1}{2}}} S_n dx = \frac{1}{4} e^{u_{ni,j}} \times \left( \frac{h_i h_j}{B\left(\frac{u_{ni-1,j} - u_{ni,j}}{2}\right) \cdot B\left(\frac{u_{ni,j} - u_{ni,j}}{2}\right)} + \frac{h_{i+1} h_j}{B\left(\frac{u_{ni+1,j} - u_{ni,j}}{2}\right) \cdot B\left(\frac{u_{ni,j} - u_{ni,j}}{2}\right)} + \frac{h_i h_{j+1}}{B\left(\frac{u_{ni-1,j} - u_{ni,j}}{2}\right) \cdot B\left(\frac{u_{ni,j} + 1 - u_{ni,j}}{2}\right)} + \frac{h_{i+1} h_{j+1}}{B\left(\frac{u_{ni+1,j} - u_{ni,j}}{2}\right) \cdot B\left(\frac{u_{ni,j} + 1 - u_{ni,j}}{2}\right)} \right). \quad (19)$$

Substituting (17) and (19) into (12), we obtain a nonlinear scheme to (10) subject to the boundary conditions for  $u_n$ .

$$\begin{aligned} & \frac{a_j}{h_{i+1}} b_n e^{u_{ni+1,j}} B(u_{ni+1,j} - u_{ni,j}) (u_{ni+1,j} - u_{ni,j}) \\ & - \frac{a_j}{h_i} b_n e^{u_{ni,j}} B(u_{ni,j} - u_{ni-1,j}) (u_{ni,j} - u_{ni-1,j}) \\ & + \frac{a_i}{h_{j+1}} b_n e^{u_{ni,j+1}} B(u_{ni,j+1} - u_{ni,j}) (u_{ni,j+1} - u_{ni,j}) \\ & - \frac{a_i}{h_j} b_n e^{u_{ni,j}} B(u_{ni,j} - u_{ni,j-1}) (u_{ni,j} - u_{ni,j-1}) \\ & - \Lambda_{i,j} u_{ni,j} = -\frac{\Lambda_{i,j}}{2} (\varphi - \varphi_n)_{i,j}. \end{aligned} \quad (20)$$

The coefficient matrix corresponding to (20) is symmetric and positive definite in a rectangular silicon region.

The QDD model was applied to simulate quantum mechanical effects of three-dimensional MOSFET structures [15]. The numerical scheme (20) is easy to extend to three dimensions and to implement into the framework of three-dimensional device simulations [16]. Moreover, this scheme is viewed as a consistent generalization of the Scharffeter–Gummel expression to the general Sturm–Liouville type equation and hence the more general formulation of the finite volume method can be applied to construct a multidimensional scheme [17].

In one dimensional case, such a nonlinear scheme was proposed by Ancona *et al.*, applying an exponential fitting method to the discretization of the nonlinear Helmholtz equation (7) to overcome a coarse grid problem in the QDD model [8]. When

comparing with the discretization scheme derived in [8], the discretization of the flux  $F$  yields a different discrete form. Indeed, one-dimensional approximation for the flux  $F_{i+1/2}$  derived in [8], where the unknown variable is  $S_n$ , reads

$$\begin{aligned} F_{i+1/2} &= \frac{1}{h_{i+1}} \frac{\sqrt{\frac{S_{ni+1}}{S_{ni}}}}{\frac{S_{ni+1}}{S_{ni}} - 1} \log\left(\frac{S_{ni+1}}{S_{ni}}\right) (S_{ni+1} - S_{ni}) \\ &= \frac{1}{h_{i+1}} \sqrt{S_{ni+1}S_{ni}} (u_{ni+1} - u_{ni}). \end{aligned} \quad (21)$$

The numerical flux  $F_{i+1/2}$  derived in [8] is obtained by the discretization of the flux (13), averaging the coefficient  $S_n$  at the cell interface by a linear approximation  $\sqrt{S_{ni+1}S_{ni}}$ . Also, one-dimensional approximation of  $\Lambda_{i,j}$  proposed in [8] reads

$$\begin{aligned} \int_{x_{i-1/2}}^{x_{i+1/2}} S_n dx &= S_{ni} \cdot \left( h_{i+1} \frac{\sqrt{\frac{S_{ni+1}}{S_{ni}} - 1}}{\log\left(\frac{S_{ni+1}}{S_{ni}}\right)} + h_i \frac{\sqrt{\frac{S_{ni-1}}{S_{ni}} - 1}}{\log\left(\frac{S_{ni-1}}{S_{ni}}\right)} \right) \\ &= \frac{S_{ni}}{2} \cdot \left( \frac{h_{i+1}}{B\left(\frac{u_{ni+1}-u_{ni}}{2}\right)} + \frac{h_i}{B\left(\frac{u_{ni-1}-u_{ni}}{2}\right)} \right) \end{aligned} \quad (22)$$

and, hence, it is found that the explicit integration of  $\Lambda_{i,j}$  derived in (19) yields an extension to two dimensions. The conservative scheme (12) constructed with (19) and (21) is also useful, which generalizes the discretization scheme proposed in [8] to multi-dimensions, if the nonlinear scheme in [8] is rewritten in terms of the new unknown variables  $u_n$ .

To obtain the full discretization schemes for the QDD equation, the current continuity equation (8) is rewritten in terms of the Slotboom variable  $\eta_n = n_i \exp(-\varphi_n)$  for the generalized chemical potential as

$$-\nabla(\mu_n e^{\varphi+\gamma_n} \nabla \eta_n) + R = 0. \quad (23)$$

The discretization for the continuity equation (23) results in the well-known Scharffeter–Gummel scheme. The numerical implementation of (10) and (23) is less sensitive to the initial solutions because of the numerical advantage of (10) and, hence, in the iterative calculation the initial guesses calculated from the DD model were applied to solve the coupled equation system without using any damping methods.

#### IV. SIMULATION RESULTS FOR MOSFET STRUCTURES

The discretization method was evaluated in a variety of MOSFET structures. Fig. 1 shows electron density distributions in the channel of a MOSFET having thin gate oxide thickness of 1.5 nm and high substrate concentration of  $1.0 \times 10^{18} \text{ cm}^{-3}$ , calculated at different gate voltages. The value of effective mass is given by a single parameter  $m_n^* = 0.26m_0$ . A computational grid, with the minimum cell of  $\sim 0.01$  nm adjacent to the silicon/oxide interface, is set up and the nonuniform grid spacing is adapted to the location of boundaries. The results are compared with those from the Schrödinger–Poisson system including 30 subbands. Since the Schrödinger–Poisson calculation includes the effect of higher subbands, there is some difference of the density distribution at bulk between

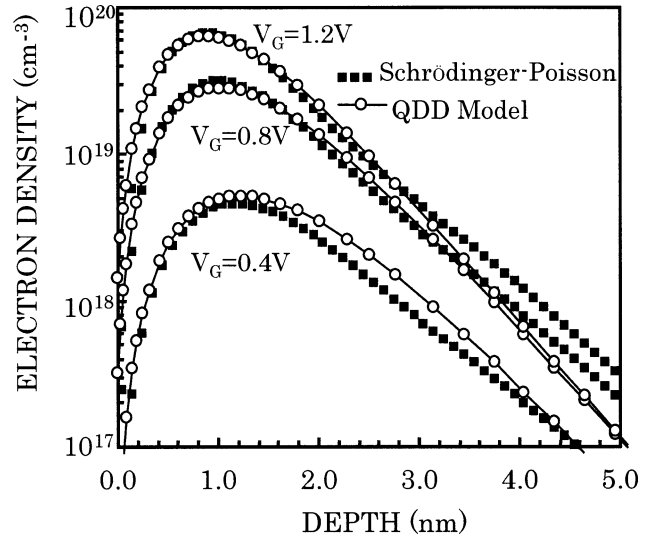


Fig. 1. Electron distributions for a MOSFET with 1.5-nm gate oxide thickness and uniform channel doping of  $1.0 \times 10^{18} \text{ cm}^{-3}$ , calculated at different gate voltages. The results are compared with those from the Poisson–Schrödinger solver.

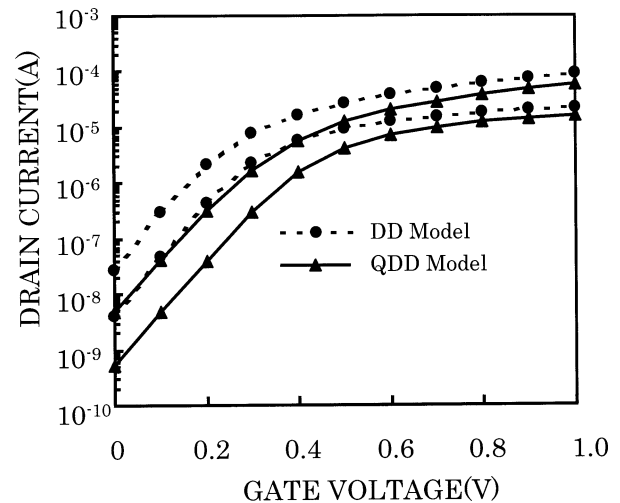


Fig. 2. Drain current versus gate voltage characteristics of a 25-nm gate length MOSFET at different drain biases,  $V_D = 0.05 \text{ V}$  and  $V_D = 0.5 \text{ V}$ . The gate oxide thickness is 1.5-nm and uniform channel doping concentration is  $2.5 \times 10^{18} \text{ cm}^{-3}$ .

the two models. As seen in Fig. 1, the surface density profiles are in good agreement between two models and the gate bias dependence of electron density is simulated well even in high substrate-doping cases. Fig. 2 shows a comparison of QDD and DD models for the drain-current versus gate-voltage characteristics of a 25-nm gate length MOSFET at different drain biases. The device has the 1.5-nm-thick gate oxide and uniform channel doping of  $2.5 \times 10^{18} \text{ cm}^{-3}$ . For the calculation of I-V characteristics, a mobility model developed for a DD model [16] was used. The high drain bias case, corresponding to  $V_D = 0.5 \text{ V}$ , is evaluated. The current-voltage characteristics at high drain biases were calculated without using any damping methods. The unbiased case is used as an initial guess and immediately the high drain bias is simulated. It is possible to give the high drain bias by a one-step increment in the iterative calculation. As expected, the comparison between these two

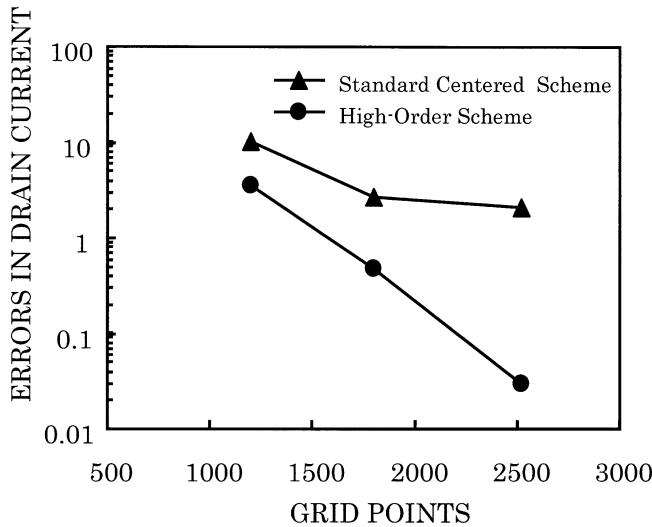


Fig. 3. Percentage errors in the drain current at gate voltage  $V_G = 0.1$  V and drain voltage  $V_D = 0.5$  V, which is plotted as a function of the number of grid points in a  $25 \times 5$  nm intrinsic region of a double gate MOSFET. Two discretization schemes are compared.

represents the threshold-voltage increase due to quantum effects in the channel, in this case by about 100 mV. It is shown that quantization in the channel degrades the subthreshold characteristics and enhances the drain-induced threshold-voltage shift. The discretization method provides numerical stability in the simulations for I-V characteristics of ultrasmall MOSFETs.

The discretization scheme (20) was further applied to simulate a double gate MOSFET with a 5-nm-thick silicon layer. The gate length is 25 nm and the gate-oxide thickness 1.5 nm. The percentage errors in the drain current are plotted in Fig. 3 as a function of the number of grid points in a  $25 \times 5$ -nm intrinsic region, comparing with exact results calculated using a fine grid with 5000 points. Two different schemes, high-order scheme (20) and standard centered scheme (12) constructed with simplified integrals (14) and (15), are compared. It is readily apparent that the high-order scheme (20) gives good accuracy in the drain current, by comparing the dependence of the errors on the number of grid points for the standard centered scheme. Fig. 4(a) and (b) demonstrates electron distributions located at the gate center of a double gate MOSFET for  $V_G = 0.1$  V and  $V_G = 0.5$  V at  $V_D = 0.1$  V, and  $V_D = 0.1$  V and  $V_D = 0.5$  V at  $V_G = 0.1$  V, comparing with those calculated from the DD model. The device has 25-nm gate length and 1.5-nm-thick gate oxide. The silicon body was doped  $10^{15}$  cm $^{-3}$   $p$ -type and a workfunction equals to the  $n^+$ -silicon. Carrier transport simulations with quantum confinement effects in a ultrathin body device are obtained from the QDD model, while the classical DD modeling yields the electron density piled up at the silicon/oxide interface in all cases. When the silicon layer decreases by 4 nm, the two inversion layers are merged even at high gate bias and the quantum confinement effect is effectively enhanced with the increase of the gate bias. The drain bias dependence of quantization in the channel is shown in Fig. 4(b). As the drain bias increases, the electron density crowded into the center of the channel decreases. This result, which is a two-dimensional effect, reveals the drain induced reduction of quantization in the channel at high drain bias.

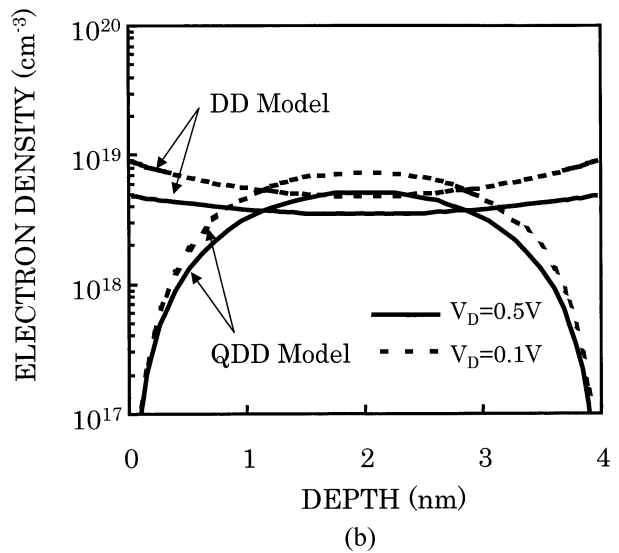
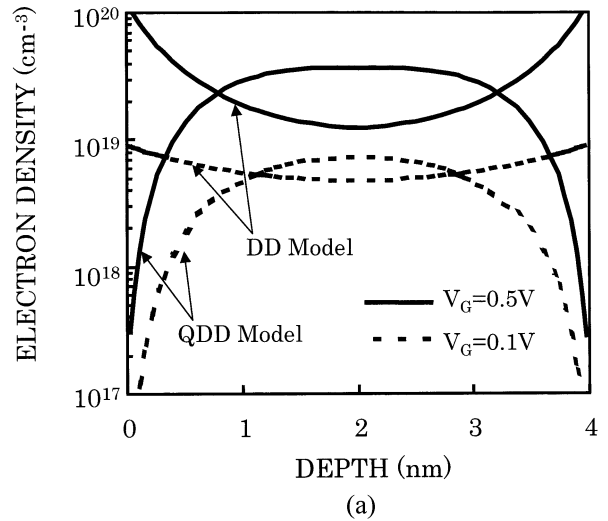


Fig. 4. (a) and (b) Electron distributions along a transverse cutline located at the gate center of a 25-nm double gate MOSFET. The device has a 4 nm thick silicon layer and 1.5-nm-thick gate oxide. The results are plotted for gate and drain bias dependence, (a)  $V_G = 0.1$  V and  $V_G = 0.5$  V at  $V_D = 0.1$  V, and (b)  $V_D = 0.1$  V and  $V_D = 0.5$  V at  $V_G = 0.1$  V.

## V. CONCLUSION

A multidimensional discretization method for the stationary QDD model has been developed and evaluated in a variety of ultrasmall MOSFET structures. The natural discretization is performed for the stationary QDD equations replaced by an equivalent form, employing the exponential transformation of variables. A conservative scheme using an exponential-fitting method is constructed in multidimensions, which leads to a consistent generalization of the Scharfetter–Gummel expression to the nonlinear Sturm-Liouville type equation. The simulation results with the discretization method are verified by those calculated from the Schrödinger equation coupling with Poisson equation and the classical drift-diffusion model. This method provides numerical stability and accuracy for carrier transport simulations with quantum confinement effects in ultrasmall MOSFET structures.

## APPENDIX

In this appendix, numerical implementation of Fermi–Dirac statistics in the discretization method considered here is discussed. For Fermi–Dirac statistics, the electron density  $n$  is approximated by introducing the band parameter  $\omega_n$  as

$$n = n_i \exp(\varphi + \gamma_n + \omega_n - \varphi_n) \quad (\text{A1})$$

where all of potentials are scaled by the Boltzmann voltage. The band parameter  $\omega_n$  is determined as

$$\omega_n = \left( \log \left( \frac{n}{N_c} \right) - G_{\frac{1}{2}} \left( \frac{n}{N_c} \right) \right) \quad (\text{A2})$$

where  $N_c$  is the density of states in the conduction band, and  $G_{1/2}$  is the inverse Fermi function of order 1/2. A convenient fit for numerical implementation, for example, is given in [18].

By employing the expression (A1) of the density, the current continuity equation of the QDD model for electrons is modified as

$$-b_n \nabla (S_n \nabla u_n) + S_n u_n = \frac{S_n}{2} (\varphi + \omega_n - \varphi_n) \quad (\text{A3})$$

$$-\nabla (\mu_n e^{\varphi + \gamma_n + \omega_n} \nabla \eta_m) + R = 0. \quad (\text{A4})$$

Equations (A2)–(A4) are self-consistently solved for numerical implementation of Fermi–Dirac statistics.

## ACKNOWLEDGMENT

The author thanks Professors T. Nogi of Kyoto University, A. Matsumura of Osaka University and A. Hiroki of Kyoto Institute of Technology for valuable discussions.

## REFERENCES

- [1] H.-S. P. Wong, "Beyond the conventional transistor," *IBM J. Res. Develop.*, vol. 46, no. 2, pp. 133–168, 2002.
- [2] M. G. Ancona and H. F. Tiersten, "Macroscopic physics of the silicon inversion layer," *Phys. Rev. B*, vol. 35, no. 15, pp. 7959–7965, 1987.
- [3] M. G. Ancona and G. J. Iafrate, "Quantum correction to the equation of state of an electron gas in a semiconductor," *Phys. Rev. B*, vol. 39, no. 13, pp. 9536–9540, 1989.
- [4] C. L. Gardner, "The quantum hydrodynamic model for semiconductor devices," *SIAM J. Appl. Math.*, vol. 54, no. 2, pp. 409–427, 1994.
- [5] M. G. Ancona, Z. Yu, R. W. Dutton, P. J. Vande Voorde, M. Cao, and V. Vook, "Density-gradient analysis of MOS tunneling," *IEEE Trans. Electron Devices*, vol. 47, pp. 2310–2319, Dec. 2000.
- [6] C. S. Rafferty, B. Biegel, Z. Yu, M. G. Ancona, J. Bude, and R. W. Dutton, "Multi-dimensional quantum effect simulation using a density-gradient model and script-level programming techniques," in *Proc. SISPAD*, Sept. 1998, pp. 137–140.
- [7] R. Pinnau and A. Unterreiter, "The stationary current-voltage characteristics of the quantum drift-diffusion model," *SIAM J. Numer. Anal.*, vol. 37, no. 1, pp. 211–245, 1999.
- [8] M. G. Ancona and B. A. Biegel, "Nonlinear discretization scheme for the density gradient equations," in *Proc. SISPAD*, Sept. 2000, pp. 196–199.
- [9] M. G. Ancona, "Finite-difference schemes for the density-gradient equations," *J. Computat. Electron.*, vol. 1, pp. 435–443, 2002.
- [10] A. Wettstein, A. Schenk, and W. Fichtner, "Quantum device simulation with density gradient model on unstructured grids," *IEEE Trans. Electron Devices*, vol. 48, pp. 279–284, Feb. 2001.
- [11] E. Lyumkis, R. Mickevicius, O. Penzin, B. Polsky, K. El Sayed, A. Wettstein, and W. Fichtner, "Simulations of ultrathin, ultrashort double-gated MOSFETs with the density gradient transport model," in *Proc. SISPAD*, Sept. 2002, pp. 271–274.
- [12] Z. Yu, R. W. Dutton, D. Yergeau, and M. G. Ancona, "Macroscopic quantum carrier transport modeling," in *Proc. SISPAD*, Sept. 2001, pp. 1–9.
- [13] G. I. Marchuk, *Methods of Numerical Mathematics*. Berlin, Germany: Springer-Verlag, 1982.
- [14] D. L. Scharfetter and H. K. Gummel, "Large signal analysis of a silicon Read diode oscillator," *IEEE Trans. Electron Devices*, vol. ED-16, pp. 64–77, Jan. 1969.
- [15] A. Asenov, G. Slavcheva, A. R. Brown, J. H. Davies, and S. Saini, "Quantum enhancement of the random dopant induced threshold voltage fluctuations in sub-100 nm MOSFETs: A 3-D density-gradient simulation study," *IEEE Trans. Electron Devices*, vol. 48, pp. 722–729, Apr. 2001.
- [16] S. Odanaka, A. Hiroki, K. Ohe, M. Moriyama, and H. Umimoto, "SMART-II: A three-dimensional CAD model for submicrometer MOSFETs," *IEEE Trans. Computer-Aided Design.*, vol. 10, pp. 619–628, May 1991.
- [17] R. E. Bank and D. J. Rose, "Some error estimates for the box method," *SIAM J. Numer. Anal.*, vol. 24, no. 4, pp. 777–787, 1987.
- [18] S. Selberherr, "MOS device modeling at 77 K," *IEEE Trans. Electron Devices*, vol. 36, pp. 1464–1474, Aug. 1989.



**Shinji Odanaka** (M'98–SM'01) received the B.S., M.S., and Ph.D. degrees in applied mathematics and physics from Kyoto University, Kyoto, Japan, in 1978, 1980, and 1991, respectively.

From 1980 to 2000, he conducted research on semiconductor process and device modeling, computer-aided design for CMOS VLSI technologies, and CMOS devices at Matsushita Electric Industrial Co., Ltd., Osaka, Japan. He pioneered three-dimensional (3-D) models for numerical process simulation in the silicon/oxide system and developed a 3-D CAD model for integrated circuit processes and devices, using a supercomputer. In 2000, he joined the Cybermedia Center, Osaka University, Osaka, Japan, where he is currently a Professor of the Computer Assisted Science Division. His research interests include numerical and mathematical modeling of semiconductor transport.

Prof. Odanaka served on several program committees of the International Electron Device Meeting from 1992 to 1993, the Symposium on VLSI Technology from 1995 to 1999, and SISPAD. He is a Member of IEICE of Japan and Japan Society of Applied Physics.